Suplemental methods

Measurement of single MT rigidity in flow experiments.

MTs are modeled as elastic rods subjected to a fluid drag (F) and constraints at both ends. We adapted the equations for an elastic filament to the experimental setup using the parameters and variables sketched in supplemental figure S5 and listed in Table 3.

Parameter	Definition	Dimensions	Typical value
L	MT (or bundle) length	L	~10 μm
r	MT (or bundle radius)	L	12.5 nm (MT only)
η	Fluid viscosity	$M.L^{-1}.T^{-1}$	~1-3×10^{-3} Pa.s
L_0	Unit length used normalization of	L	1 μm
kT	Thermal energy	$M.L^2.T^{-2}$	4.1×10^{-21} J
$N_0=(kT/L_0)$	Unit force	$M.L.T^{-2}$	4.1×10^{-15} N
κ	Flexural rigidity		
C_T	Drag per unit length	$M.L^{-1}.T^{-1}$	~10^{-3} Pa.s
	$C_T = (2\pi\eta/(\ln(L/2r)-0.2))$		
V (V_x, V_y)	Fluid velocity (horizontal and vertical components of velocity)	$L.T^{-1}$	~ 40-60 μm.s^{-1}
α	$\alpha = (N_0 L_0^{\,2}/\kappa)$	-	10^{-3}
β	$\beta = (C_T L_0^2/N_0)$	T	~0.45 s.
Variables			
s	Arc-length normalized by L_0	-	
(x, y)	Normalized position of a point in the MT	-	
(N_x, N_y)	Normalized internal elastic force	-	
θ	Angle between the unit tangent vector and the horizontal axis.	-	

Table 3. Parameters and variables used in equations and in the determination of MT

(or bundles of MT) rigidity.

From the inextensibility condition of the MT, the balance of force and moment we get the set of differential equations which can be numerically solved

$$\frac{dx}{ds} = \cos\theta$$
$$\frac{dy}{ds} = \sin\theta$$
$$\frac{d^2\theta}{ds^2} = \alpha\left(-N_x \sin\theta + N_y \cos\theta\right) \qquad \text{Eq. 1}$$
$$\frac{dN_x}{ds} = -\beta\left[\left(1+\sin^2\theta\right)V_x - \cos\theta\sin\theta V_y\right]$$
$$\frac{dN_y}{ds} = -\beta\left[-\cos\theta\sin\theta V_x + \left(1+\cos^2\theta\right)V_y\right]$$

MT inextensibility is represented by the first two equations; the third equation expresses the balance between bending and the force moment. Force balance between the internal force and the external drag give the last two equations**.** Boundary conditions for the extremities are (i) at *s=0*, the MT is fixed to the pattern, so that its position and angle are also fixed

$$x(0) = x_0,$$
$$y(0) = y_0 \qquad \text{Eq.2}$$
$$\theta(0) = \theta_0.$$

(ii) at *s=L*, the MT end is free and, therefore, no forces nor momentum are applied to it

$$N_x(L) = 0,$$
$$N_y(L) = 0, \qquad \text{Eq. 3}$$
$$\left(\frac{d\theta}{ds}\right)_{s=L} = 0.$$

Solutions of Eq. 1-3 depend on the ratio (α/β) only. In consequence, we use the expression of the drag coefficient CT (table 1) so that the only remaining unknown parameters is MT (or bundle) rigidity. Given the position of the MT points and orientations (x, y and θ), its length and the velocity of the fluid (V_x and V_y), we apply

the following algorithm to determine the MT(bundle) rigidity.

Measurement of MT/bundle flexibility using fluctuations.

Conformations of MTs or bundles of MTs undergoing thermal fluctuations are extracted from time lapse movies every 20 sec. The filament contour shape is approximated by a superposition of Fourier modes (n=8). At equilibrium, the equipartition theorem ensures that each mode contributes an average energy of $(kT/2)$ (Gittes et al., The Journal of Cell Biology, 1993, 120, 923-934). This implies that the flexural rigidity is given by the statistical distribution of the Fourier amplitudes as (see Gittes et al., The Journal of Cell Biology, 1993, 120, 923-934)

$$\kappa = \frac{kT}{Var(a_n)}\left(\frac{L}{n\pi}\right)^2$$

where $Var(a_n)$ is the variance of the amplitudes of the n^{th} Fourier mode; L is the MT(bundle) length. Note that each mode provides an independent estimate of the rigidity.

Bundle orientation in the flow and prediction of bundle flexural rigidities.

The flexural rigidities of bundle configurations shown in Figure S6 were computed using the standard definition of the bending modulus for a MT

$$\kappa_0 = EI_0,$$

where E is the Young modulus of the tubulin lattice (assuming continuous distribution of the mass) and I_0 is the second moment of area of the MT. The expression of this moment is

$$I_0 = \frac{\pi\left(r_e^2 - r_i^2\right)}{4},$$

where r_e (resp. r_i) is the external (resp. internal) MT radius. Fortunately, the Huygens theorem is helpful in the derivation of other configurations flexural rigidities, as listed in the Table 4.

	Bundle configuration	Flexural rigidity ratio	Range
Single MT		$\kappa_0 = E\frac{\pi\left(r_e^4 - r_i^4\right)}{4}$	-
Bundle of 2 MT	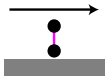	2	2
	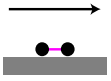	$2+\frac{4h^2}{r_e^2+r_i^2}$	~ 42-51
Bundle of 3 MT	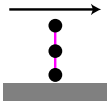	3	3
	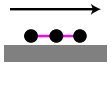	$3+\frac{8h^2}{r_e^2+r_i^2}$	~ 84-101
	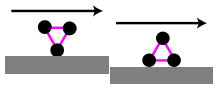	$3+\frac{4h^2}{r_e^2+r_i^2}$	~ 43-52

Table 4. Flexural rigidity of microtubule bundle configurations (measured in units of flexural rigidity for a single microtubule, first row). r_e (resp. r_i) is the external (resp. internal) microtubule radius; h is the center-to-center microtubule distance. We used r_e=12.5 nm, r_i= 9.5 nm. Assuming that the length of a MAP dimer connecting two

microtubules is in the range 25 to 30 nm, we conclude that h is in the range 50 to 55 nm.

Supporting Figure legends:

Figure S1. Protein purification and measurement of MAP65 apparent Kd

(A-E). For each MAP65, the Coomassie-stained SDS-PAGE gel of the purified recombinant His-MAP65 and His-MAP65-GFP is shown on the left, and the data corresponding to the measurements of the apparent kD are shown on the right. For MAP65-1, MAP65-4, Chimera 1-4, and MAP65-1(MBD), the data were graphed as the concentration of His-MAP65-GFP bound to MTs in function of the unbound His-MAP65-1-GFP concentration. For Ase1, the data were graphed as the concentration of His-Ase1-GFP in function of total tubulin concentration. **(F).** Table summarizing the different apparent Kd determined for the various MAP65 and constructs used in this study.

Figure S2. Predicted Lp for different bundle configurations and orientations.

Schematic representation of different bundles formed by two or three MTs that are bent in a flow. Only two orientations of bundles relative to the fluid flow are sketched. The letter in bracket gives the bundle configuration and the Lp is expressed as a multiplicative factor of single MT Lp. The predicted Lp is based on the assumption that both the angle of the bond along the MT lattice and the bond length are constant during bundle deformation. The angle and the bond length are, respectively, 60° and 30 nm for MAP65-1 (31) and 90° and 15 nm for MAP65-4 (32). For Ase1, only the length bond (6 nm) is determined (Schuyler et al., 2003,, data not shown).

Figure S3. Encountering event distribution of individual MTs in presence of MAP65

(A). Time-lapses of single MTs elongating from MT seeds in the presence of GFP-MAP65-1 (50 nM) and Alexa-561 labeled tubulin (22 μM), observed by TIRF microscopy (left). MTs are in red, MAP65-1 in green. The three MT outcomes

observed are represented: bundling (top panel), cross-over (middle panel), and touch-and-run (bottom panel). Arrowheads indicate the growing ends of collide MTs that encounter resident MTs. Schemes on the right panel illustrate the different MT outcomes observed in the assay. MTs are in red with their minus ends marked by a red disc and their dynamic ends by black arrows. **(B, C).** Histograms represent the frequencies of crossing (B) and (C) touch and run events between two individual MTs as a function of their angle of interaction and of MT polarity in presence of 50 nM MAP65-1, Ase1, MAP65-4 and Chimera 1-4 (with range of ten degrees, from 0° to 90°). Red and blue bars correspond respectively to anti-parallel and parallel interactions between MTs. Encountering frequencies are the ratio of co-aligned MTs over the total number of encountering events. **(D).** Table of the frequencies of the three outcomes observed between MTs that are classified according to the MT encounter angle and the MT polarity.

Figure S4. Encountering event distribution of MT bundles induced by MAP65

(A). Time-lapses of MT bundled MTs elongating from MT seed bundles in the presence of GFP-MAP65-1, MAP65-1 and Chimera 1-4 (50 nM) and Alexa-561 labeled tubulin (22 μM) and that co-align in order to generate a thicker MT bundle (left). MTs are in red, MAP65 in green. Schemes on the right panel illustrate the bundling outcomes in presence of the different MAP65. Arrowheads indicate the growing ends of collide MT bundles that encounter resident MT bundles. **(B-C).** Histograms of encountering frequencies after crossing (A) and (B) touch-and-run events between MT bundles as a function of the interaction angles of MT bundles (with range of ten degrees, from 0° to 90°). **(C).** Table of the frequencies of the three outcomes observed between MT bundles (bundling, crossing, touch-and-run) that are classified according to the bundle encounter angle.

Figure S5. Examples of MT co-alignment, buckling and deformation in presence of MAP65-1

(A-C). Time-lapses of individual MTs or MT bundles elongating from MT seeds in the presence of GFP-MAP65-1 (100 nM) and Alexa-568-labeled tubulin (22 μM), observed by TIRF microscopy. MTs are in red, MAP65-1 in green. Scale bar: 5 μm**.**

Figure S6. Variables and parameters used in the model.

(A-B). Schematic representation of a MT (or a bundle of MTs) in the resting configuration (dotted red line) or bent by the flow (solid red line). The position of any point along the filament is determined either by its arc-length, s, or by its Cartesian coordinates (x(s), y(s)). In addition, we define θ(s) the angle between the horizontal axis and the unit vector tangent to the filament (blue arrow, panel A). The flow velocity (red arrow, panel B) exerts a force, denoted by F (magenta arrow, panel B) all over along the filament. Since the filament is at rest in the moving fluid, the elastic force developed in the filament, denoted by N (black arrow), balances the force exerted by the fluid.

The boundary conditions used in the model are indicated at both filament ends (panel A). Fixing the MTs to the pattern imposes the position and the orientation of the MTs at one end (panel A). At the other the MT end, which is not bound to the pattern, the elastic force and bending should vanish (panel A).

Movies

Movie S1. Lp determination of single MTs growing from a MT seed, aligned on a functionalized bar pattern. MTs are in green, MT seeds and beads in red. The MT is bent as described in Figure 1. Time is in minutes and seconds. Bar: 10 μm.

Movie S2. Lp determination of single MTs growing in presence of 100 nM MAP65-1. MTs are in green, MT seeds and beads in red. The MT is bent as described in Figure 1. Time is in minutes and seconds. Bar: 10 μm.

Movie S3. Lp determination of a MT bundle growing in presence of 100 nM Ase1. MTs are in green, MT seeds and beads in red. MT bundles are bent as described in Figure 3. Time is in minutes and seconds. Bar: 10 μm.

Movie S4. Lp determination of a MT bundle growing in presence of 100 nM MAP65-4. MTs are in green, MT seeds and beads in red. MT bundles are bent as described in Figure 3. Time is in minutes and seconds. Bar: 10 μm.

Movie S5. Encountering events of individual MTs (Alexa-568-labeled tubulin) in the absence of MAPs (left movie), or in the presence of 50 nM GFP-MAP65-1 (middle movie) and GFP-Ase1 (right movie). MTs are in red, MAP65-1/Ase1 in green. Time is in minutes and seconds. Bar: 10 μm.

Movie S6. Example of a cross-over event between two elongating individual MTs (Alexa-568-labeled tubulin) in presence of 50 nM GFP-MAP65-1. MTs are in red, MAP65-1 in green. Arrows indicate the MT end that collides with a MT. Time is in minutes and seconds. Bars: 5 μm.

Movie S7. Example of a touch-and-run event between two elongating individual MTs (Alexa-568-labeled tubulin) in presence of 50 nM GFP-MAP65-1. MTs are in red, MAP65-1 in green. Arrows indicate the MT end that collides with a MT. Time is in minutes and seconds. Bar: 5 μm.

Movie S8. Example of a zippering event between two elongating individual MTs (Alexa-568-labeled tubulin) in presence of 50 nM GFP-MAP65-1. MTs are in red, MAP65-1 in green. Arrows indicate the MT end that collides with a MT. Time is in minutes and seconds. Bar: 5 μm.

Figure S1

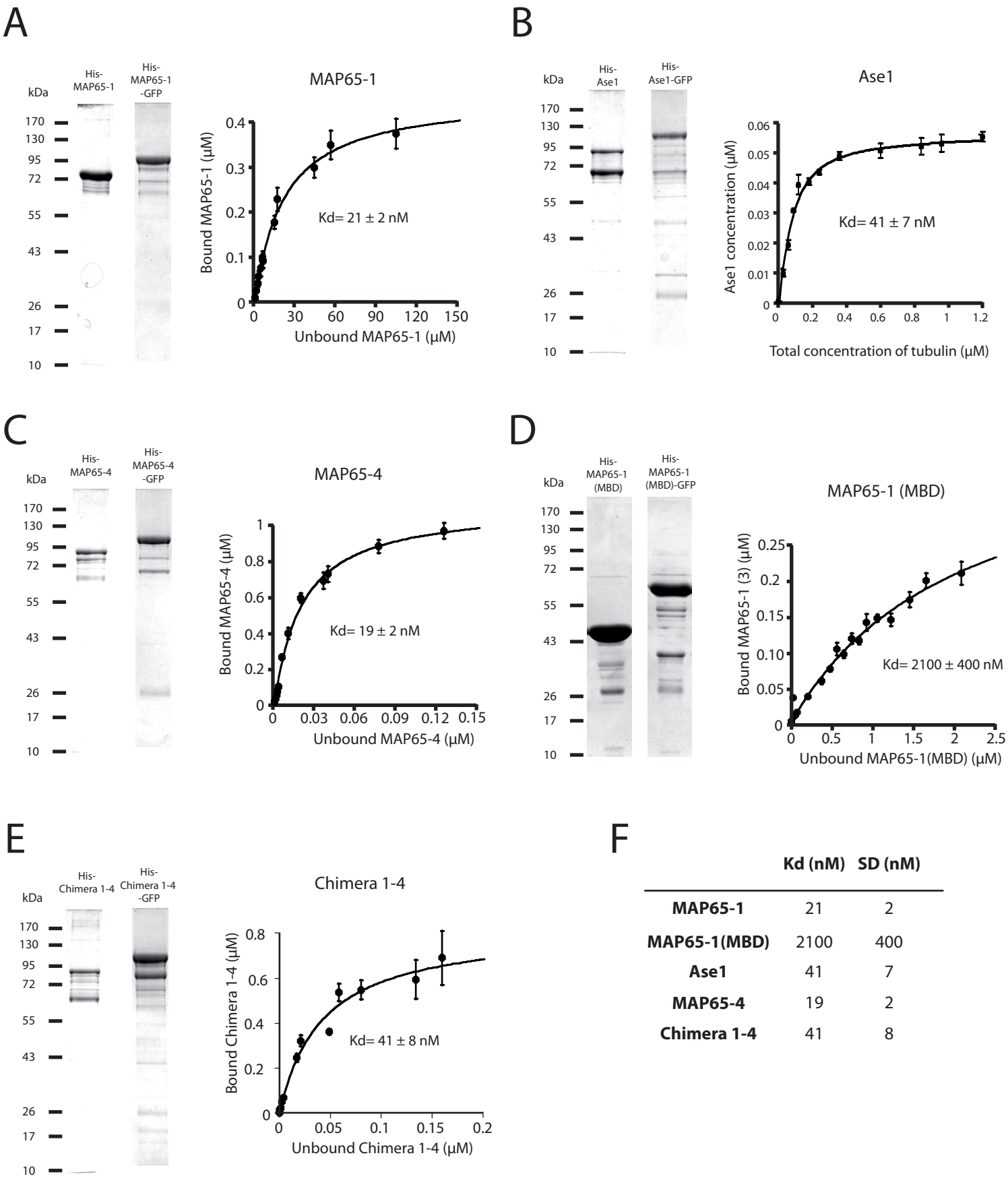

F

	Kd (nM)	SD (nM)
MAP65-1	21	2
MAP65-1(MBD)	2100	400
Ase1	41	7
MAP65-4	19	2
Chimera 1-4	41	8

Figure S2

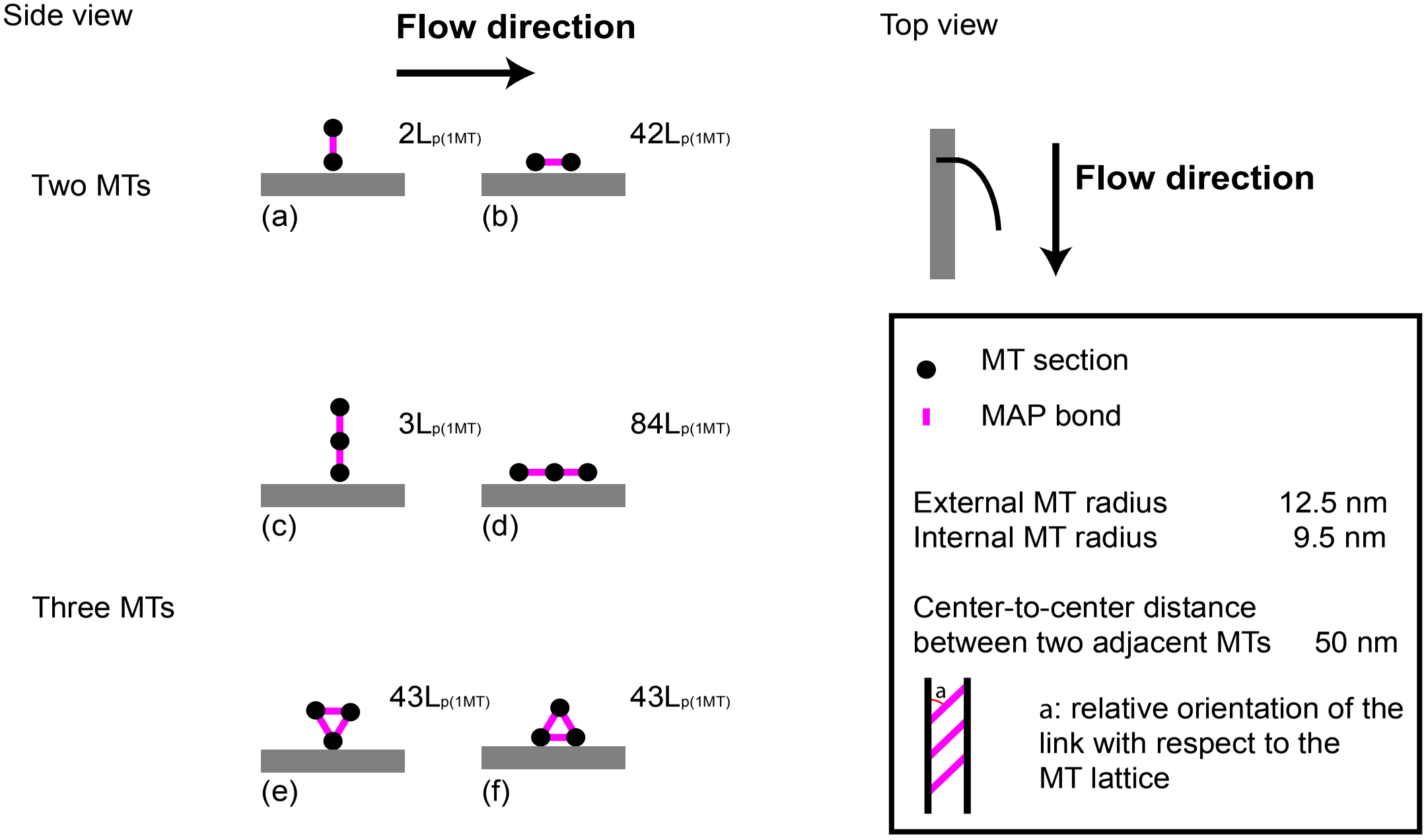
Side view
Flow direction
Top view
Two MTs
2Lp(1MT)
42Lp(1MT)
(a)
(b)
Flow direction
3Lp(1MT)
84Lp(1MT)
(c)
(d)
Three MTs
43Lp(1MT)
43Lp(1MT)
(e)
(f)
MT section
MAP bond
External MT radius 12.5 nm
Internal MT radius 9.5 nm
Center-to-center distance
between two adjacent MTs 50 nm
a
a: relative orientation of the
link with respect to the
MT lattice

Figure S3

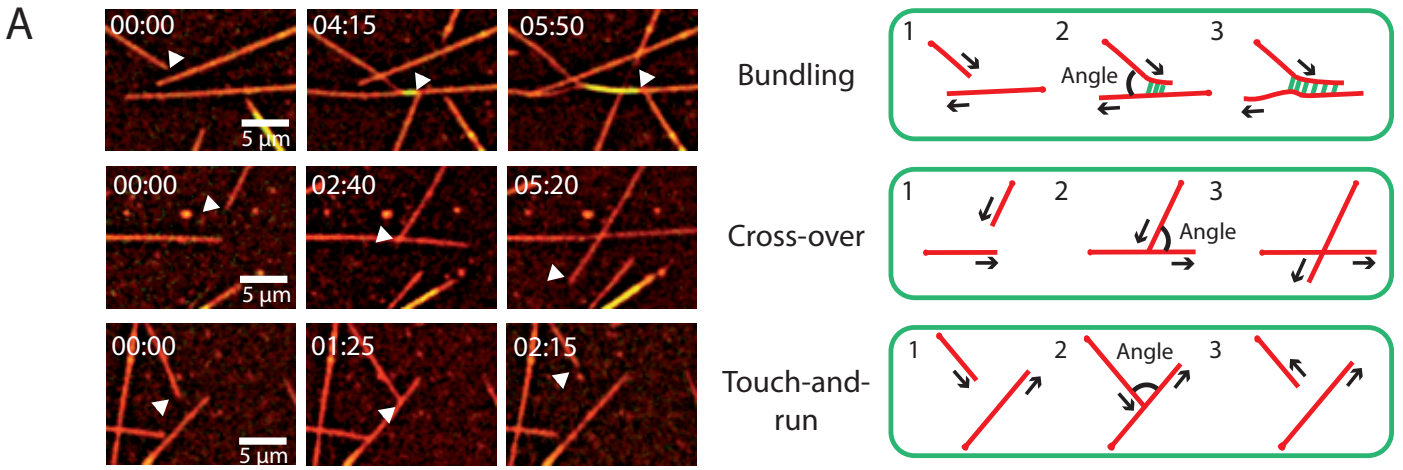

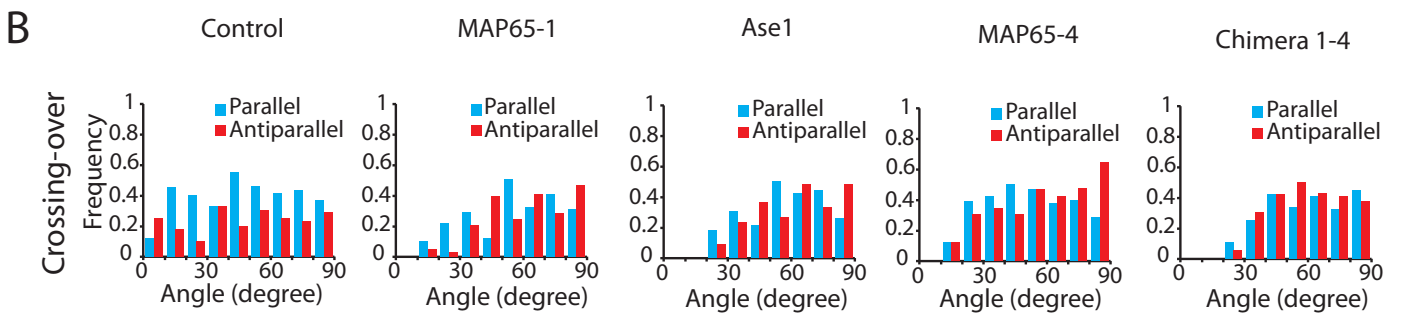

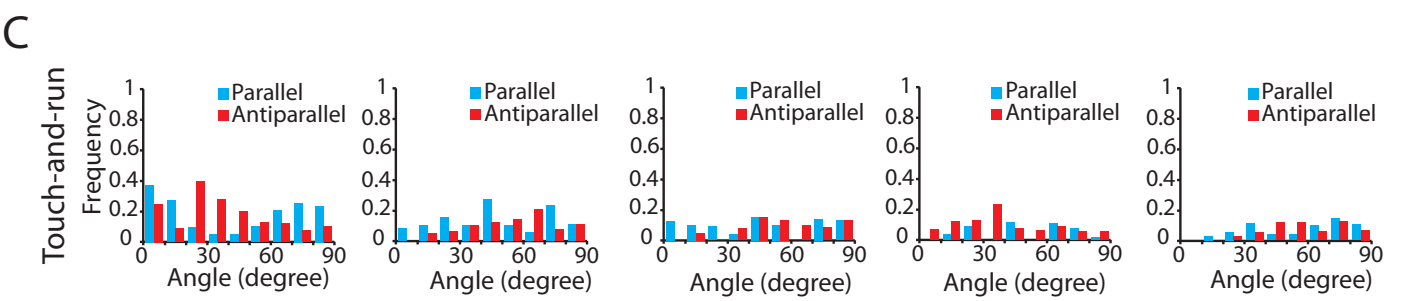

D

	Type of encountering events	Number	Bundling Max angle	Bundling frequency	Cross-over frequency	Touch-and-run frequency
Control	Polar	122	0	0.0%	39.4%	18.4%
	Anti-polar	84	0	0.0%	23.8%	18.4%
MAP65-1	Polar	141	27	3.3%	25.4%	13.6%
	Anti-polar	171	45	24.8%	23.2%	9.7%
Ase1	Polar	99	16	3.6%	25.8%	9.7%
	Anti-polar	138	45	27.8%	25.0%	8.0%
MAP65-4	Polar	143	18	9.0%	32.9%	5.0%
	Anti-polar	172	22	8.9%	34.3%	9.9%
Chimera 1-4	Polar	176	36	15.7%	25.6%	6.9%
	Anti-polar	188	39	17.7%	27.8%	6.3%

Figure S4

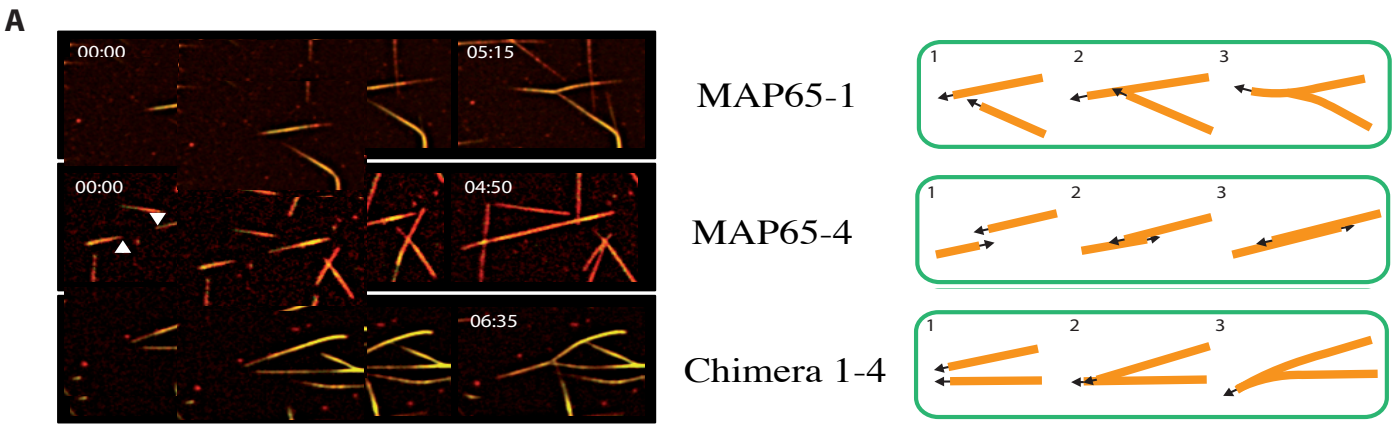

D

	Number	Bundling Max angle	Bundling frequency	Cross-over frequency	Touch-and-run frequency
MAP65-1	237	45	43.9%	46.1%	10.0%
Ase1	190	45	42.9%	49.3%	7.7%
MAP65-4	220	25	17.3%	69.8%	12.9.7%
Chimera 1-4	189	25	26.3%	66.7%	7.0%

Figure S5

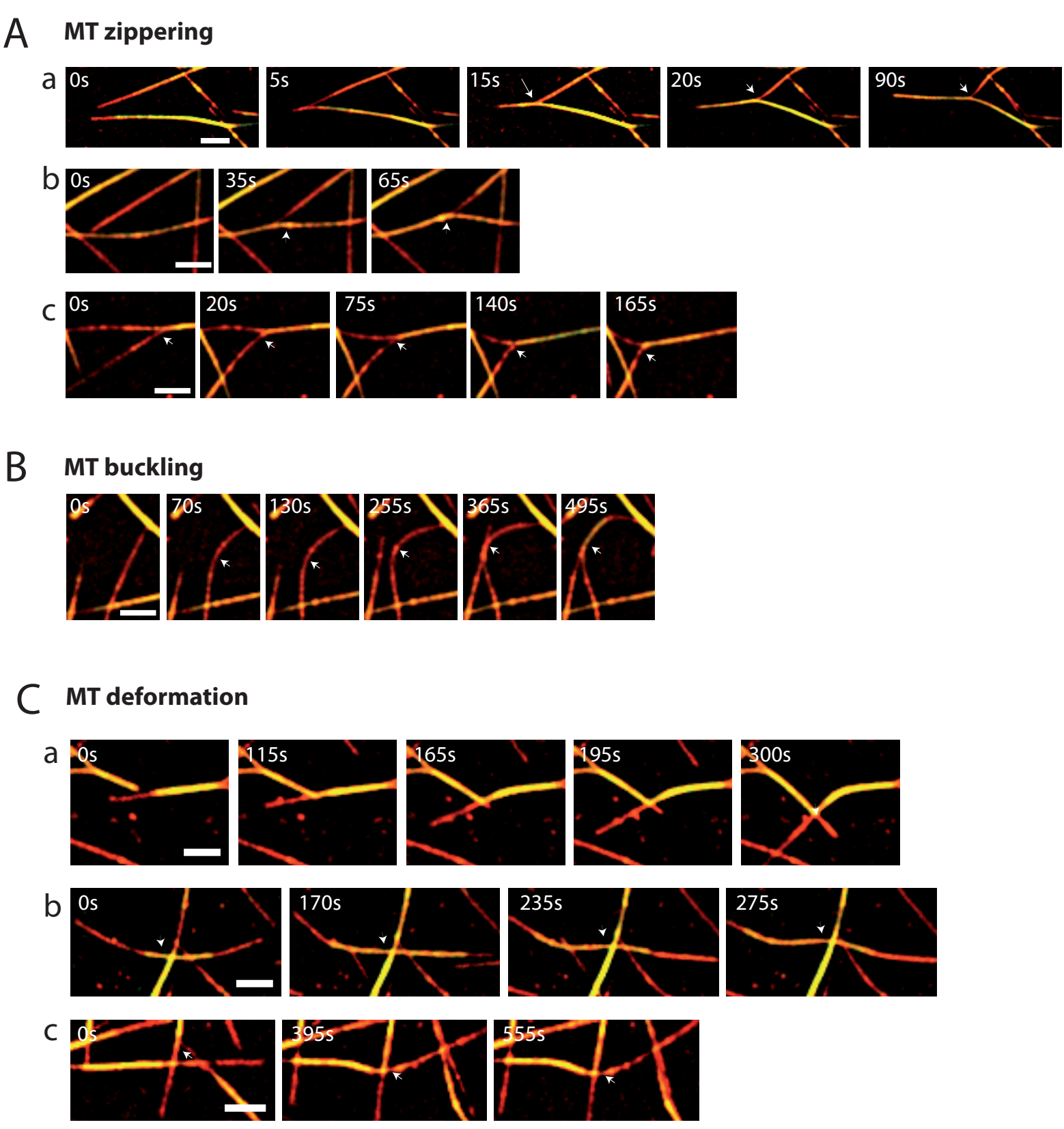
A
MT zippering
a
0s
5s
15s
20s
90s
b
0s
35s
65s
c
0s
20s
75s
140s
165s
B
MT buckling
0s
70s
130s
255s
365s
495s
C
MT deformation
a
0s
115s
165s
195s
300s
b
0s
170s
235s
275s
c
0s
395s
555s

Figure S6